Letter

Collective dynamics in active polar polymer assemblies

Hossein Vahid,[1] Jens-Uwe Sommer,[1,2,*] and Abhinav Sharma[3,1,†]

[1]*Bereich Theorie der Polymere, Leibniz-Institut für Polymerforschung Dresden, 01069 Dresden, Germany*

[2]*Institut für Theoretische Physik, Technische Universität Dresden, 01069 Dresden, Germany*

[3]*Institute of Physics, University of Augsburg, Faculty of Mathematics, Natural Sciences, and Materials Engineering, Universitätsstraße 1, 86159 Augsburg, Germany*

(Received 2 April 2025; accepted 9 October 2025; published 5 November 2025)

Tangentially driven active polymers, model systems for motor-driven filaments, have been extensively studied in uniform activity fields. Here, we show that an activity gradient breaks fore-aft symmetry, generating net body forces that steer dimers, asters, and larger assemblies toward high-activity regions. Including temporal stochasticity softens the chains, allowing them to bend and wind around other filaments. Once several contacts are established, steric interlocking arrests relative motion and stabilizes the assembly into a hierarchically entangled cluster. These clusters persist for times far exceeding single-chain relaxation and do not appear under deterministic, temporally constant activity. Remarkably, such activity-induced gelation occurs even at polymer concentrations substantially lower than those typically required for passive chains. Our results reveal a mechanism for activity-induced aggregation, providing strategies for designing autonomous and reconfigurable microfluidic systems.

DOI: 10.1103/g369-z3hn

Introduction. Polymer chains propelled tangentially along their backbone provide a framework for studying emergent behavior of active wormlike chains and motor-driven filaments [1–13]. Previous studies have largely focused on weakly interacting polymers in homogeneous and time-independent activity fields, where individual chains evolve from straight to spiral or globular conformations as activity increases [6,10,11,14–16], and collectively, transition from jamming at low activity to nematic order at intermediate levels, and active turbulence at high activity [17]. However, biological systems often feature spatially and temporally varying energy input, leading to pronounced structural complexity, including aggregation, entanglement, and gelation [18–22].

We demonstrate that spatial activity gradients and temporal propulsion noise induce the formation of nonequilibrium entangled structures between assemblies of tangentially driven active polymers (TDAPs) at concentrations well below those required for passive polymers. Single TDAPs accumulate in low-activity regions without entangling. In contrast, activity gradients bias outward-driven dimers, asters, and larger assemblies toward high-activity regions, and the temporal stochasticity in propulsion increases conformational flexibility, allowing polymers to bend, loop, and interlock. The resulting aggregates are stabilized purely by entanglements, without any adhesive bonds or attractive interactions. Compared with spatially uniform activity, an activity gradient accelerates entanglement nucleation and increases aggregate persistence.

The model. We perform Brownian dynamics simulations to investigate semiflexible TDAPs and multiarm TDAPs [see Figs. 1(a) and 1(b)]. Each TDAP monomer experiences a self-propulsion force $\boldsymbol{F}_{\mathrm{a}}^{i} = f_{\mathrm{a}}\boldsymbol{e}^{i}$, where f_{a} is the magnitude of the active force and $\boldsymbol{e}^{i}$ denotes the unit vector indicating the propulsion direction. The propulsion direction of each monomer (except for the polymer ends) at position $\boldsymbol{r}^{i}$ is aligned with the local tangent vector of the polymer backbone, updated at each time step by $\boldsymbol{e}^{i}(t) = \boldsymbol{t}^{i}/|\boldsymbol{t}^{i}|$, where $\boldsymbol{t}^{i} = \boldsymbol{r}^{i+1} - \boldsymbol{r}^{i-1}$, and $\boldsymbol{r}^{i-1}$ and $\boldsymbol{r}^{i+1}$ represent the positions of the adjacent monomers. For the first and last monomers of the chains, $\boldsymbol{e}^{i}$ aligns with the bond connecting them to their nearest-neighbor monomers.

The equation of motion of each monomer is described by $\gamma_{\mathrm{t}}\dot{\boldsymbol{r}}^{i} = -\sum_{j}\nabla_{\boldsymbol{r}^{i}}U^{ij} + \boldsymbol{F}_{\mathrm{a}}^{i} + \boldsymbol{\xi}^{i}(t)$, where γ_{t} is the translational friction coefficient of particle i and U is the potential energy. The stochastic noise $\boldsymbol{\xi}^{i}(t)$ is Gaussian, with zero mean $\langle\boldsymbol{\xi}^{i}(t)\rangle = 0$ and autocorrelation function $\langle\xi_{\alpha}^{i}(t).\xi_{\beta}^{j}(t')\rangle = 2\gamma_{\mathrm{t}}^{-1}k_{\mathrm{B}}T\delta^{ij}\delta_{\alpha\beta}\delta(t-t')$, where k_{B} is the Boltzmann constant, T is the temperature, and $\alpha, \beta \in \{x, y, z\}$. Interparticle interactions are modeled using the Weeks-Chandler-Andersen (WCA) potential [23], $U_{\mathrm{WCA}}^{ij}(r) = 4\epsilon[(\frac{\sigma^{ij}}{r^{ij}})^{12} - (\frac{\sigma^{ij}}{r^{ij}})^{6} + \frac{1}{4}]\Theta(r_{\mathrm{c}}^{ij} - r^{ij})$, where r^{ij} is the distance between particles i and j, and $\sigma^{ij} = 0.5(\sigma^{i} + \sigma^{j})$ is their effective interaction diameter, with σ^{i} being the diameter of particle i. Here, ϵ is the depth of the potential well, Θ is the Heaviside step function, and the cutoff radius is set to $r_{\mathrm{c}}^{ij} = 2^{1/6}\sigma^{ij}$. In addition to WCA interactions, the bonded

*Contact author: jens-uwe.sommer@tu-dresden.de

†Contact author: abhinav.sharma@uni-a.de

Published by the American Physical Society under the terms of the Creative Commons Attribution 4.0 International license. Further distribution of this work must maintain attribution to the author(s) and the published article's title, journal citation, and DOI.

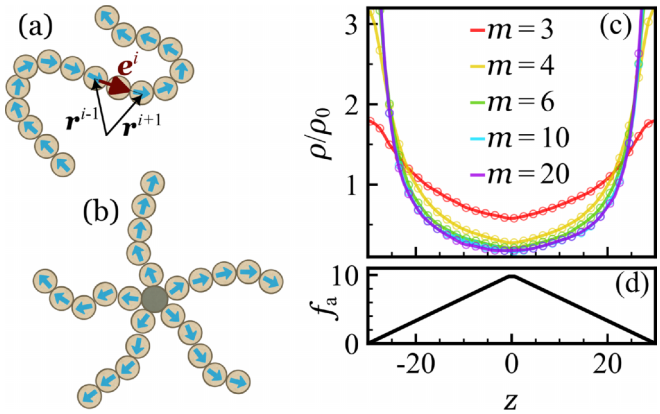

FIG. 1. Cartoon representation of (a) a TDAP and (b) an aster. Each active monomer is self-propelled in the direction of the local tangent to the backbone as indicated by the blue arrows. (c) Steady-state density of monomers along the z axis for varying degrees of polymerization m. The bulk monomer density is $\rho_0 = 0.002$. Polymers are simple TDAPs as in panel (a), and the activity field is given by $f_a = 10(1 - |z|/30)$ [see panel (d)]. TDAPs accumulate in the low-activity regions.

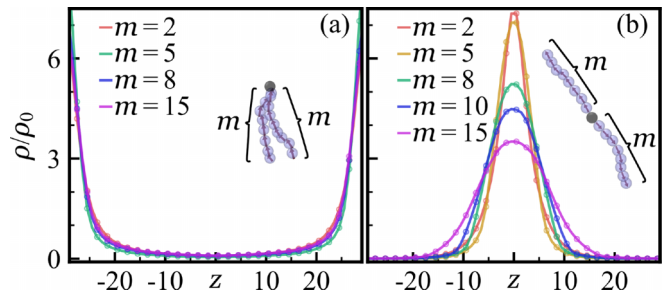

FIG. 2. Steady-state density of monomers along the z axis. Polymers have two symmetric TDAP arms, each containing m monomers, connected to a passive core, with $\rho_0 = 0.002$. $f_a(z)$ follows that of Fig. 1(d). (a) TDAPs are directed toward the core and accumulate in the low-activity regions. (b) TDAPs are directed away from the core and migrate to high-activity regions.

monomers are connected using the finite extensible nonlinear elastic potential [24], defined as $U_F(r) = -\frac{1}{2}k_F R_0^2 \ln[1 - (\frac{r^{ij}}{R_0})^2]\Theta(R_0 - r^{ij})$, where k_F represents the elastic coefficient and R_0 is the maximum bond length. The chain conformation is controlled by the bending potential $U_b = k_b[1 - \cos(\theta - \theta_0)]$, where k_b is the bending modulus, θ is the angle between consecutive bonds, and θ_0 is the rest angle.

We set $\sigma = 1$, $\epsilon = k_B T = 1$, and $\tau = \sigma^2\gamma_t/(3k_B T)$, with $\gamma_t = 3$, as the units of length, energy, and time, respectively. All simulations are conducted using the LAMMPS package [25,26] within a cubic simulation box of dimensions $60 \times 60 \times 60\sigma^3$, ranging from -30 to 30 along each axis. Periodic boundary conditions are imposed in all directions. The activity field varies linearly along the z axis according to $f_a(z) = f_a^*(1 - |z|/30)$, where $f_a = f_a^*$ at the box center $z = 0$ and $f_a = 0$ at $|z| = 30$. In a subset of simulations, we impose temporal stochasticity on the activity field. To this end, the box is partitioned along z into slabs of width 0.5. At each time step, an independent uniform random variate $\eta(z, t) \in [0, 1]$ is drawn for each slab, and the local activity is updated as $f_a(z, t) = f_a(z)\,\Theta[P - \eta(z, t)]$. Here, $P \in [0, 1]$ is a control parameter setting the activation probability (mean duty cycle); thus, the local activity of the slab equals $f_a(z)$ with probability P and 0 otherwise. The simulation parameters are set to $\sigma^i = 1$, $k_F = 30$, $R_0 = 2\sigma^i$, $k_b = 30$, and $\theta_0 = 120°$. Additional computational details are described in the Supplemental Material [27].

Results. We first study individual TDAP chains in an activity field given by $f_a = 10(1 - |z|/30)$. Figure 1(c) shows that these polymers tend to accumulate in low-activity regions, regardless of the chain length. TDAP propulsion aligns with the polymer backbone, and thus, following the motions of their head monomers, TDAP chains preferentially orient and accumulate toward lower-activity regions. Including temporal stochasticity does not alter the single-arm TDAP response. They still accumulate in low-activity regions, with only a slight increase as P increases (cf. Fig. S3 of the Supplemental Material [27]). In contrast, active Brownian polymers (ABPOs) exhibit length-dependent accumulation and migrate to high-activity regions as the degree of polymerization m increases [33–36] (cf. Fig. S1 of the Supplemental Material [27]). Monomeric active Brownian particles (ABPs) and dimers favor low-activity regions, and at sharp motility gradients, Janus microswimmers polarize from high to low activity so that their density in regions is set by the local activities [33,37,38]. Temporal switching does not qualitatively change the ABPO response. At very low P, the mean propulsion is too weak to sense the gradient, reducing drift and accumulation in the high-activity region (Fig. S3 of the Supplemental Material [27]).

In many biological systems, active filaments are observed in assembled structures, such as bundles and asters [39–49]. Figure 2 shows that the directed motion and the overall conformation of two connected TDAPs are significantly influenced by their relative propulsion directions. We connect two TDAP arms, each consisting of m monomers, to a central passive core. We consider two distinct configurations: inward-directed [tangential propulsion from the arm tips toward the core, Fig. 2(a)] and outward-directed [from the core toward the arm tips, Fig. 2(b)]. In the inward-directed case, the two arms tend to approach each other, which again leads to accumulation in lower-activity regions. Inward propulsion creates effective inward-directed stresses leading to arm folding at the core position that stabilizes their collective migration toward low activity. Variations in m do not significantly influence this behavior.

For outward-directed propulsion, the two arms exhibit a tug-of-war dynamics [50]. The tug-of-war of motor proteins was also found to be highly cooperative and perform directed cargo transport [51]. Here, tangential propulsion extends the chain, and the arm sampling the higher-activity side experiences the larger thrust; the resulting net force points up the gradient, leading to drift and accumulation in the high-activity region. This behavior corresponds to rigid ABP dimers exhibiting polarity-dependent accumulation. In this case, it was shown analytically that the outward-oriented dimers migrate to high-activity regions, whereas the inward-oriented dimers accumulate in low-activity regions [52]. Figure 2 shows that

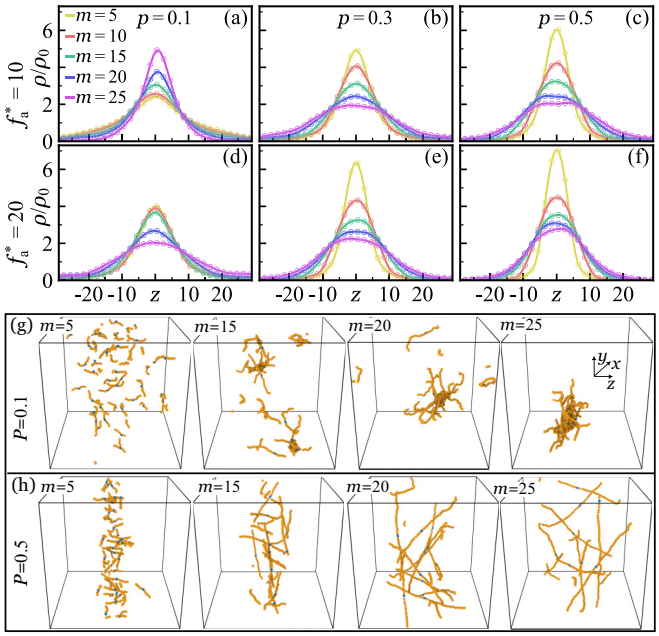

FIG. 3. Steady-state monomer density along the z axis for varying P and m for two-arm outward-directed TDAP assemblies. The activity field is given by $f_a = f_a^*(1 - |z|/30)\Theta[P - \eta(z,t)]$: (a), (c) $f_a^* = 10$ and (d), (f) $f_a^* = 20$. Bulk density of monomers is $\rho_0 = 0.002$. Each polymer has two symmetric arms (m monomers each) attached to a passive core. Panels (g) and (h) show representative snapshots of the systems in panels (a) and (c), respectively. TDAPs are colored yellow and the cores are blue. Movies S1–S4 of Supplemental Material [27] show the simulation animations at $f_a^* = 5$, 10, and 20.

as arm length increases, monomers tend to accumulate in high-activity regions more, but their spatial distribution becomes broader, and the peak density at the highest activity decreases. Since the polymer remains nearly stretched, not all monomers can occupy the same z position. While the core remains in the high-activity region (see Fig. S6 of the Supplemental Material [27]), the extended arms reach lower-activity areas. Furthermore, our results show that as the polymer becomes more stretched (increasing θ_0) or stiffer (increasing k_b), the accumulation in the high-activity regions enhances (cf. Fig. S8 of the Supplemental Material [27]). In biological systems, cross-linked actin and microtubule (MT) structures often exhibit asymmetric arm lengths [19]. Increasing asymmetry eventually leads to accumulation in low-activity regions. Interestingly, at intermediate asymmetry, polymers accumulate in the intermediate-activity regions due to the competition between arms (cf. Fig. S9 of the Supplemental Material [27]).

Figure 3 demonstrates how stochastic activity (activation probability P) and the maximum propulsion strength f_a^* control the collective organization and spatial distribution of two-arm, outward-directed TDAP assemblies. For short chains (e.g., $m = 5$), increasing either f_a^* or P enhances the tug-of-war between the arms, leading to enhanced accumulation in high-activity regions. Unexpectedly, long chains (e.g., $m = 25$) at low P and low f_a^* become flexible and entangle into stable, asterlike aggregates [panel (g)]. The longer the

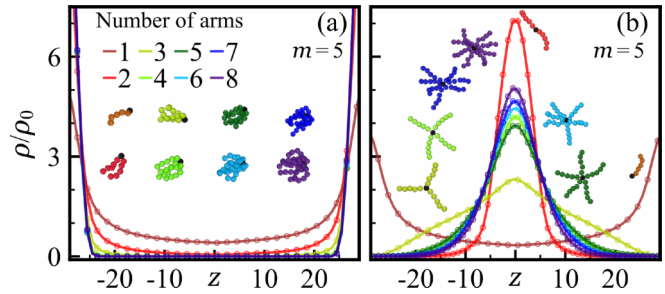

FIG. 4. Steady-state density of monomers along the z axis for polymers with varying numbers of arms. Each arm is an (a) inward- or (b) outward-directed TDAP with five monomers. The activity field is given by $f_a = 10(1 - |z|/30)$, and the bulk monomer density is set to $\rho_0 = 0.002$.

chain, the more stable the entangled structures (cf. Movies S1–S4 of the Supplemental Material [27]). Increasing P or f_a^* stiffens the arms, suppresses entanglement, and permits extended conformations, so the peak density decreases. Bond-vector autocorrelations confirm this trend, decaying more rapidly for small P (cf. Fig. S7 of the Supplemental Material [27]). No persistent entanglement is observed in the deterministic limits $P = 1$ (always on) or $P = 0$ (always off). Once steady state is established, inverting the gradient (i.e., $f_a(z) = 10|z|/30$) translates the preformed aggregate toward the maximum; transiently detached filaments reassociate in the high-activity region (Movie S4 of the Supplemental Material [27]).

Figure 4 presents multiarm stars, each containing five monomers ($m = 5$) extending from a central passive core. Such multiarm geometries are common in cytoskeletal networks and cellular assemblies [53,54]. Recent experiments showed control over inward- and outward-directed forces on MTs using light-switchable motors [55] or by balancing motor activity and polymerization [19]. Mixed active-passive polymers have also been realized experimentally in kinesin-driven MT-actin composites [56]. We examine inward-directed propulsion [toward the central core, Fig. 4(a)] and outward-directed propulsion [away from the core, Fig. 4(b)]. For inward-directed propulsion, arms tend to collapse close to each other, forming compact, bundlelike structures. These arms cooperatively move toward the low-activity region, and increasing the number of arms enhances accumulation in that region.

For outward-directed propulsion, the polymer unfurls into an aster that migrates toward the high-activity region, yet the drift strength is nonmonotonic in arm number. Maximum accumulation in the high-activity region is achieved for the two-arm structure, which decreases dramatically when a third arm is added. Here, the three-arm polymer faces competition among arms oriented toward different activity levels, reducing the net directional migration. Increasing the number of arms to four slightly improves accumulation relative to the three-arm structure. Further increases in arm number have minimal effects. These trends are robust to variations in f_a^* and bulk densities of monomers (ρ_0) (see Fig. S13 of the Supplemental Material [27]). At very high densities, accumulation extends to lower-activity regions because the high-activity regions

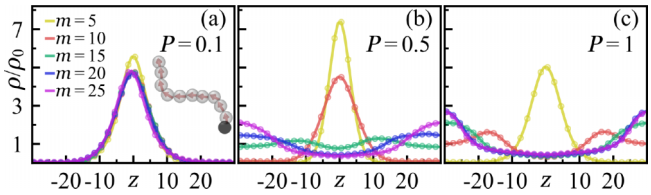

FIG. 5. Steady-state monomer density along the z axis for varying P and m. The activity field is given by $f_a = 5(1 - |z|/30)\Theta[P - \eta(z,t)]$. Each polymer consists of a TDAP pulling an attractive cross-linker particle. Panel (a) includes an overlaid schematic of a TDAP with $m = 10$ (gray spheres), pulling a cross-linker (black sphere). Movie S5 of Supplemental Material [27] illustrates animations of simulations at varying m and P.

become saturated. For longer arms ($m > 15$), the density profiles become nearly arm-number independent (Fig. S12 of the Supplemental Material [27]). Multiarm ABPOs also accumulate in high-activity regions, and both increasing the number of arms and m enhance their accumulation (Fig. S12 of the Supplemental Material [27]). We note that two outward-directed arms are sufficient to bias migration toward the high-activity region, irrespective of the polarity of the remaining arms (cf. Fig. S11 of the Supplemental Material [27]).

Cytoskeletal assemblies can emerge spontaneously, for example, through motor-driven reorganization, filament buckling, and cross-linking interactions [18,44,57–66]. To simulate dynamic assemblies, we consider TDAPs that each pull a passive cross-linker attached at the tail. The cross-linkers interact attractively with one another via a Lennard-Jones potential with well depth $\epsilon = 15$ (see Eq. (S3) of the Supplemental Material [27]), and all other interactions are described by the WCA potential, thus forming temporal asters with outward-directed activity of the arms. The activity field is $f_a(z,t) = 5(1 - |z|/30)\Theta[P - \eta(z,t)]$. Figure 5 presents the steady-state monomer density profiles for varying m and P. At low P (e.g., $P = 0.1$), attraction dominates over active forces and TDAPs form asters that accumulate in high-activity regions (cf. Movie S5 of the Supplemental Material [27]). At $m = 5$, many small asters appear, and increasing m yields fewer, larger aggregates. At the largest chain length considered ($m = 25$), a single large aggregate forms, with individual TDAP chains dynamically exchanging between the aggregate and the surrounding region. The aggregates accumulate in the high-activity regions (cf. Movie S5 of the Supplemental Material [27]).

As P increases, the competition between the chain activity and cross-linker attraction determines the structural stability and accumulation pattern of TDAPs. Short chains ($m = 5$) remain largely aggregated in asters across P, with slightly reduced stability at $P = 1$. Thus, accumulation in the high-activity region slightly decreases at $P = 1$. Longer chains ($m \geqslant 10$) are more sensitive to activity. At intermediate P (e.g., $P = 0.5$), polymers with $m = 10$ still form stable asters, allowing pronounced accumulation in high-activity regions. Further increasing P leads to the formation of transient structures: Asters initially assemble and move toward higher activity, but active forces eventually dominate, causing them to dissociate. This results in density peaks at intermediate positions along the gradient. For even longer polymers, attractive forces fail to stabilize aggregates at high P, resulting in the dispersal of individual chains to low-activity regions.

To confirm the generality and robustness of our findings, we systematically explored how varying polymer conformation, activity magnitude, polymer concentration, the degree of partial activation, and confinement affect the observed behaviors (see the Supplemental Material [27]). Across these variations, our results remain consistent, demonstrating the generality of the observed behaviors.

Conclusions. In uniform activity, directed transport of active polymers is strongly coupled to polymer configuration and structure [10,11,14–16,34]. Compact structures exhibit reduced mobility, whereas elongated configurations exhibit enhanced diffusion and directed motion [6,11,67]. The coupling can be tuned by where activity is placed along the backbone and even by partial activation, which can induce knots [68] and improve transport efficiency [12]. We have shown that stochastic activity enhances the accumulation of long polymer assemblies ($m > 20$) in high-activity regions.

In this Letter, we have demonstrated that spatial and temporal variations in activity can fundamentally transform the collective behavior of TDAPs. Our findings show that (1) structured assemblies with at least two outward-driven arms robustly migrate to high-activity regions, regardless of whether the remaining arms are passive, inward-, or outward-driven. (2) Introducing stochasticity in the activity field enhances two- and multiarm TDAP flexibility and leads to spontaneous formation of entangled clusters that are absent in deterministic systems. (3) Attractive cross-linkers attached to the tails of TDAP can stabilize dynamic aggregates of long TDAPs in high-activity regions, in particular when combined with temporally stochastic activity. The resulting structure, ranging from persistent asters to transient clusters or dispersed chains, depends on the interplay between chain length, propulsion strength, and linker affinity, which together determine whether polymers accumulate in high-, intermediate-, or low-activity regions.

Our findings could be experimentally tested using microtubule gliding assays [69,70] and synthetic swimmers [71]. Light patterns and light-controlled motor activation have also been used to generate and transport MT [55,72] and actin [19,22] assemblies such as asters, providing a potential method to explore the dynamics and stability of assemblies in inhomogeneous activity fields.

Acknowledgments. We thank Michael Lang for the discussions. This work was supported by Deutsche Forschungsgemeinschaft (DFG) under Projects No. 561963765 (H.V.) and No. 525864799 (A.S.). J.U.S. thanks the cluster of excellence "Physics of Life" at TU Dresden for its support. We gratefully acknowledge the NHR Center at TU Dresden for providing high-performance computing resources.

Data availability. The data that support the findings of this article are openly available [73].

[1] Z. Mokhtari and A. Zippelius, Dynamics of active filaments in porous media, Phys. Rev. Lett. **123**, 028001 (2019).

[2] R. Sinaasappel, M. Fazelzadeh, T. Hooijschuur, Q. Di, S. Jabbari-Farouji, and A. Deblais, Locomotion of active polymerlike worms in porous media, Phys. Rev. Lett. **134**, 128303 (2025).

[3] V. Schaller, C. Weber, C. Semmrich, E. Frey, and A. R. Bausch, Polar patterns of driven filaments, Nature (London) **467**, 73 (2010).

[4] G. De Canio, E. Lauga, and R. E. Goldstein, Spontaneous oscillations of elastic filaments induced by molecular motors, J. R. Soc. Interface **14**, 20170491 (2017).

[5] S. K. Anand and S. P. Singh, Structure and dynamics of a self-propelled semiflexible filament, Phys. Rev. E **98**, 042501 (2018).

[6] V. Bianco, E. Locatelli, and P. Malgaretti, Globulelike conformation and enhanced diffusion of active polymers, Phys. Rev. Lett. **121**, 217802 (2018).

[7] C. A. Philipps, G. Gompper, and R. G. Winkler, Tangentially driven active polar linear polymers—An analytical study, J. Chem. Phys. **157**, 194904 (2022).

[8] J.-X. Li, S. Wu, L.-L. Hao, Q.-L. Lei, and Y.-Q. Ma, Nonequilibrium structural and dynamic behaviors of polar active polymer controlled by head activity, Phys. Rev. Res. **5**, 043064 (2023).

[9] M. Fazelzadeh, E. Irani, Z. Mokhtari, and S. Jabbari-Farouji, Effects of inertia on conformation and dynamics of tangentially driven active filaments, Phys. Rev. E **108**, 024606 (2023).

[10] C. Karan, A. Chaudhuri, and D. Chaudhuri, Inertia and activity: Spiral transitions in semi-flexible, self-avoiding polymers, Soft Matter **20**, 6221 (2024).

[11] H. Khalilian, F. Peruani, and J. Sarabadani, Structural dynamics and optimal transport of an active polymer, Soft Matter **20**, 7592 (2024).

[12] M. Vatin, S. Kundu, and E. Locatelli, Conformation and dynamics of partially active linear polymers, Soft Matter **20**, 1892 (2024).

[13] M. A. Ubertini, E. Locatelli, and A. Rosa, Universal time and length scales of polar active polymer melts, ACS Macro Lett. **13**, 1204 (2024).

[14] R. E. Isele-Holder, J. Elgeti, and G. Gompper, Self-propelled worm-like filaments: Spontaneous spiral formation, structure, and dynamics, Soft Matter **11**, 7181 (2015).

[15] C. Zhao, R. Yan, and N. Zhao, Collective behavior of active filaments with homogeneous and heterogeneous stiffness, J. Chem. Phys. **161**, 154901 (2024).

[16] L. van Steijn, M. Fazelzadeh, and S. Jabbari-Farouji, Conformation and dynamics of wet externally actuated filaments with tangential active forces, Phys. Rev. E **110**, 064504 (2024).

[17] Ö. Duman, R. E. Isele-Holder, J. Elgeti, and G. Gompper, Collective dynamics of self-propelled semiflexible filaments, Soft Matter **14**, 4483 (2018).

[18] J. Prost, F. Jülicher, and J.-F. Joanny, Active gel physics, Nat. Phys. **11**, 111 (2015).

[19] M. Schuppler, F. C. Keber, M. Kröger, and A. R. Bausch, Boundaries steer the contraction of active gels, Nat. Commun. **7**, 13120 (2016).

[20] E. Demir, Y. I. Yaman, M. Basaran, and A. Kocabas, Dynamics of pattern formation and emergence of swarming in *Caenorhabditis elegans*, eLife **9**, e52781 (2020).

[21] A. Deblais, K. R. Prathyusha, R. Sinaasappel, H. Tuazon, I. Tiwari, V. P. Patil, and M. S. Bhamla, Worm blobs as entangled living polymers: From topological active matter to flexible soft robot collectives, Soft Matter **19**, 7057 (2023).

[22] R. Zhang, S. A. Redford, P. V. Ruijgrok, N. Kumar, A. Mozaffari, S. Zemsky, A. R. Dinner, V. Vitelli, Z. Bryant, M. L. Gardel *et al.*, Spatiotemporal control of liquid crystal structure and dynamics through activity patterning, Nat. Mater. **20**, 875 (2021).

[23] J. D. Weeks, D. Chandler, and H. C. Andersen, Role of repulsive forces in determining the equilibrium structure of simple liquids, J. Chem. Phys. **54**, 5237 (1971).

[24] R. B. Bird, C. F. Curtiss, R. C. Armstrong, and O. Hassager, *Dynamics of Polymeric Liquids* (Wiley, New York, 1987).

[25] S. Plimpton, Fast parallel algorithms for short-range molecular dynamics, J. Comput. Phys. **117**, 1 (1995).

[26] A. P. Thompson, H. M. Aktulga, R. Berger, D. S. Bolintineanu, W. M. Brown, P. S. Crozier, P. I. Veld, A. Kohlmeyer, S. G. Moore, T. D. Nguyen, R. Shan, M. J. Stevens, J. Tranchida, C. Trott, and S. J. Plimpton, LAMMPS—A flexible simulation tool for particle-based materials modeling at the atomic, meso, and continuum scales, Comput. Phys. Commun. **271**, 108171 (2022).

[27] See Supplemental Material at http://link.aps.org/supplemental/10.1103/g369-z3hn for additional results and simulation animations, which includes Refs. [28–32].

[28] L. Martínez, R. Andrade, E. G. Birgin, and J. M. Martínez, PACKMOL A package for building initial configurations for molecular dynamics simulations, J. Comput. Chem. **30**, 2157 (2009).

[29] A. I. Jewett *et al.*, Moltemplate a tool for coarse-grained modeling of complex biological matter and soft condensed matter physics, J. Mol. Biol. **433**, 166841 (2021).

[30] A. Stukowski *et al.*, Visualization and analysis of atomistic simulation data with OVITO-the Open Visualization Tool, Model. Simul. Mater. Sci. Eng. **18**, 015012 (2009).

[31] F. L. Memarian, J. D. Lopes, F. J. Schwarzendahl, M. G. Athani, N. Sarpangala, A. Gopinathan, D. A. Beller, K. Dasbiswas, and L. S. Hirst, Active nematic order and dynamic lane formation of microtubules driven by membrane-bound diffusing motors, Proc. Natl. Acad. Sci. USA **118** (2021).

[32] L. Huber, R. Suzuki, T. Krüger, E. Frey, and A. R. Bausch, Emergence of coexisting ordered states in active matter systems, Science **361**, 255 (2018).

[33] H. D. Vuijk, H. Merlitz, M. Lang, A. Sharma, and J.-U. Sommer, Chemotaxis of cargo-carrying self-propelled particles, Phys. Rev. Lett. **126**, 208102 (2021).

[34] S. Ravichandir, B. Valecha, P. L. Muzzeddu, J.-U. Sommer, and A. Sharma, Transport of partially active polymers in chemical gradients, Soft Matter **21**, 1835 (2025).

[35] P. L. Muzzeddu, A. Gambassi, J.-U. Sommer, and A. Sharma, Migration and separation of polymers in nonuniform active baths, Phys. Rev. Lett. **133**, 118102 (2024).

[36] B. Valecha, H. Vahid, P. L. Muzzeddu, J.-U. Sommer, and A. Sharma, Active transport of cargo-carrying and interconnected chiral particles, Soft Matter **21**, 3384 (2025).

[37] N. A. Söker, S. Auschra, V. Holubec, K. Kroy, and F. Cichos, How activity landscapes polarize microswimmers without alignment forces, Phys. Rev. Lett. **126**, 228001 (2021).

[38] S. Auschra, V. Holubec, N. A. Söker, F. Cichos, and K. Kroy, Polarization-density patterns of active particles in motility gradients, Phys. Rev. E **103**, 062601 (2021).

[39] P. A. Nguyen, A. C. Groen, M. Loose, K. Ishihara, M. Wühr, C. M. Field, and T. J. Mitchison, Spatial organization of cytokinesis signaling reconstituted in a cell-free system, Science **346**, 244 (2014).

[40] K. Ishihara, P. A. Nguyen, A. C. Groen, C. M. Field, and T. J. Mitchison, Microtubule nucleation remote from centrosomes may explain how asters span large cells, Proc. Natl. Acad. Sci. USA **111**, 17715 (2014).

[41] Z. Feng, A. Caballe, A. Wainman, S. Johnson, A. F. Haensele, M. A. Cottee, P. T. Conduit, S. M. Lea, and J. W. Raff, Structural basis for mitotic centrosome assembly in flies, Cell **169**, 1078 (2017).

[42] J. B. Woodruff, B. F. Gomes, P. O. Widlund, J. Mahamid, A. Honigmann, and A. A. Hyman, The centrosome is a selective condensate that nucleates microtubules by concentrating tubulin, Cell **169**, 1066 (2017).

[43] G. D. Gupta and L. Pelletier, Centrosome biology: Polymer-based centrosome maturation, Curr. Biol. **27**, R836 (2017).

[44] S. R. Norris, S. Jung, P. Singh, C. E. Strothman, A. L. Erwin, M. D. Ohi, M. Zanic, and R. Ohi, Microtubule minus-end aster organization is driven by processive HSET-tubulin clusters, Nat. Commun. **9**, 2659 (2018).

[45] M. Soares e Silva, M. Depken, B. Stuhrmann, M. Korsten, F. C. MacKintosh, and G. H. Koenderink, Active multistage coarsening of actin networks driven by myosin motors, Proc. Natl. Acad. Sci. USA **108**, 9408 (2011).

[46] F. Huber, D. Strehle, and J. Käs, Counterion-induced formation of regular actin bundle networks, Soft Matter **8**, 931 (2012).

[47] M. Bovellan, Y. Romeo, M. Biro, A. Boden, P. Chugh, A. Yonis, M. Vaghela, M. Fritzsche, D. Moulding, R. Thorogate *et al.*, Cellular control of cortical actin nucleation, Curr. Biol. **24**, 1628 (2014).

[48] M. Fritzsche, D. Li, H. Colin-York, V. Chang, E. Moeendarbary, J. Felce, E. Sezgin, G. Charras, E. Betzig, and C. Eggeling, Self-organizing actin patterns shape membrane architecture but not cell mechanics, Nat. Commun. **8**, 14347 (2017).

[49] H. Colin-York, D. Li, K. Korobchevskaya, V. T. Chang, E. Betzig, C. Eggeling, and M. Fritzsche, Cytoskeletal actin patterns shape mast cell activation, Commun. Biol. **2**, 93 (2019).

[50] P. L. Muzzeddu, H. D. Vuijk, H. Löwen, J.-U. Sommer, and A. Sharma, Active chiral molecules in activity gradients, J. Chem. Phys. **157**, 134902 (2022).

[51] M. J. Müller, S. Klumpp, and R. Lipowsky, Tug-of-war as a cooperative mechanism for bidirectional cargo transport by molecular motors, Proc. Natl. Acad. Sci. USA **105**, 4609 (2008).

[52] H. D. Vuijk, S. Klempahn, H. Merlitz, J.-U. Sommer, and A. Sharma, Active colloidal molecules in activity gradients, Phys. Rev. E **106**, 014617 (2022).

[53] C. A. Weber, R. Suzuki, V. Schaller, I. S. Aranson, A. R. Bausch, and E. Frey, Random bursts determine dynamics of active filaments, Proc. Natl. Acad. Sci. USA **112**, 10703 (2015).

[54] C. P. Brangwynne, G. H. Koenderink, F. C. MacKintosh, and D. A. Weitz, Cytoplasmic diffusion: Molecular motors mix it up, J. Cell Biol. **183**, 583 (2008).

[55] L. M. Lemma, M. Varghese, T. D. Ross, M. Thomson, A. Baskaran, and Z. Dogic, Spatio-temporal patterning of extensile active stresses in microtubule-based active fluids, PNAS Nexus **2**, pgad130 (2023).

[56] J. Berezney, B. L. Goode, S. Fraden, and Z. Dogic, Extensile to contractile transition in active microtubule–actin composites generates layered asters with programmable lifetimes, Proc. Natl. Acad. Sci. USA **119**, e2115895119 (2022).

[57] C. Hentrich and T. Surrey, Microtubule organization by the antagonistic mitotic motors kinesin-5 and kinesin-14, J. Cell Biol. **189**, 465 (2010).

[58] D. Gordon, A. Bernheim-Groswasser, C. Keasar, and O. Farago, Hierarchical self-organization of cytoskeletal active networks, Phys. Biol. **9**, 026005 (2012).

[59] M. E. Tanenbaum, R. D. Vale, and R. J. McKenney, Cytoplasmic dynein crosslinks and slides anti-parallel microtubules using its two motor domains, elife **2**, e00943 (2013).

[60] T. H. Tan, M. Malik-Garbi, E. Abu-Shah, J. Li, A. Sharma, F. C. MacKintosh, K. Keren, C. F. Schmidt, and N. Fakhri, Self-organized stress patterns drive state transitions in actin cortices, Sci. Adv. **4**, eaar2847 (2018).

[61] G. Henkin, W.-X. Chew, F. Nédélec, and T. Surrey, Cross-linker design determines microtubule network organization by opposing motors, Proc. Natl. Acad. Sci. USA **119**, e2206398119 (2022).

[62] B. Najma, W.-S. Wei, A. Baskaran, P. J. Foster, and G. Duclos, Microscopic interactions control a structural transition in active mixtures of microtubules and molecular motors, Proc. Natl. Acad. Sci. USA **121**, e2300174121 (2024).

[63] C. Utzschneider, B. Suresh, A. Sciortino, J. Gaillard, A. Schaeffer, S. Pattanayak, J.-F. Joanny, L. Blanchoin, and M. Théry, Force balance of opposing diffusive motors generates polarity-sorted microtubule patterns, Proc. Natl. Acad. Sci. USA **121**, e2406985121 (2024).

[64] B. Lemma, N. P. Mitchell, R. Subramanian, D. J. Needleman, and Z. Dogic, Active microphase separation in mixtures of microtubules and tip-accumulating molecular motors, Phys. Rev. X **12**, 031006 (2022).

[65] Y. H. Tee, T. Shemesh, V. Thiagarajan, R. F. Hariadi, K. L. Anderson, C. Page, N. Volkmann, D. Hanein, S. Sivaramakrishnan, M. M. Kozlov *et al.*, Cellular chirality arising from the self-organization of the actin cytoskeleton, Nat. Cell Biol. **17**, 445 (2015).

[66] K. Matsuda, W. Jung, Y. Sato, T. Kobayashi, M. Yamagishi, T. Kim, and J. Yajima, Myosin-induced F-actin fragmentation facilitates contraction of actin networks, Cytoskeleton **81**, 339 (2024).

[67] N. Jain and S. Thakur, Collapse dynamics of chemically active flexible polymer, Macromolecules **55**, 2375 (2022).

[68] M. Vatin, E. Orlandini, and E. Locatelli, Upsurge of spontaneous knotting in polar diblock active polymers, Phys. Rev. Lett. **134**, 168301 (2025).

[69] E. C. V R, E. C. S. Kloth, F. Nisini, C. Reuther, and S. Diez, Lowering ionic strength improves the sensitivity of microtubule gliding assay based molecular detection, Nano Lett. **25**, 8194 (2025).

[70] R. Catalano, Y. Zhao, M. Pecak, T. Korten, and S. Diez, Barcoding microtubules: Encoding information onto macromolecules by photobleaching, Nano Lett. **25**, 5283 (2025).

[71] Y. Ji, X. Lin, Z. Wu, Y. Wu, W. Gao, and Q. He, Macroscale chemotaxis from a swarm of bacteria-mimicking nanoswimmers, Angew. Chem. **58**, 12200 (2019).

[72] T. D. Ross, H. J. Lee, Z. Qu, R. A. Banks, R. Phillips, and M. Thomson, Controlling organization and forces in active matter through optically defined boundaries, Nature (London) **572**, 224 (2019).

[73] H. Vahid, J.-U. Sommer, and A. Sharma, Supporting data for "Collective dynamics in active polar polymer assemblies", Zenodo (2025), https://doi.org/10.5281/zenodo.17313455.